

A Neutral Voltage Modulation Strategy For Cascaded Multilevel Inverters Under Unbalance DC Sources

R S Kathirvel¹, J.Nagaraju², S.Venkatrao³

^{2,3} Assistant professor, Dept of EEE

^{1,2,3}Sri Venkatesa Perumal College Of Engineering &Technology.

Abstract- This paper proposes a pulse width-modulation strategy to achieve balanced line-to-line output voltages and to maximize the modulation index in the linear modulation range where the output voltage can be linearly adjusted in the multilevel cascaded inverter (MLCI) operating under unbalanced dc-link conditions. In these conditions, the linear modulation range is reduced, and a significant output voltage imbalance may occur as voltage references increase. In order to analyze these effects, the voltage vector space for MLCI is evaluated in detail. From this analysis, the theory behind the output voltage imbalance is explained, and the maximum linear modulation range considering an unbalanced dc-link condition is evaluated. After that, a neutral voltage modulation strategy is proposed to achieve output voltage balancing as well as to extend the linear modulation range up to the maximum reachable point in theory. In the proposed method, too large of a dc-link imbalance precludes the balancing of the output voltages. This limitation is also discussed. Both the simulations and the experiments for a seven-level phase-shifted modulated MLCI for electric vehicle traction motor drive show that the proposed method is able to balance line-to-line output voltages as well as to maximize the linear modulation range under the unbalanced dc-link conditions

Keywords- Multilevel cascaded invert-ers(MLCIs), neutral voltage modulation (NVM), phase-shifted (PS) modulation, space vector pulsewidth modulation (PWM) (SVPWM).

I. INTRODUCTION

MULTILEVEL inverters enable the synthesis of a sinusoidal output voltage from several steps of voltages. For this reason, multilevel inverters have low dv/dt characteristics and generally have low harmonics in the output voltage and current. In addition, the switching of very high voltages can be achieved by stacking multilevel inverter modules. Due to these advantages, multilevel inverters have been applied in various application fields. Among various topologies for multilevel inverters, the multilevel cascaded inverter (MLCI) structure is one of the prominent topologies because of its simple structure for modularization and fault-tolerant capability. Therefore, MLCIs are used for many applications, such as dynamic

voltage restorer, static synchronous compensator (STATCOM), high-voltage energy storage device, photovoltaic inverters, medium-voltage drives, electric vehicle (EV) traction drives, and so on . In MLCI applications, a modulation strategy to generate gating signals is very crucial to achieve high-performance control. Regarding this issue, many studies have been conducted, and they are roughly categorized into multilevel selective harmonic elimination pulse width modulation (PWM) (SHEPWM), multilevel carrier-based PWM, and multilevel space vector PWM (SVPWM) methods. Generally, a carrier-based PWM or SVPWM is preferred in applications such as motor drives , where dynamic properties are very important, whereas SHEPWM is preferred in some high-power static power conversion applications. In, an SVPWM method has been studied to cover the vermodulation range in the multilevel inverter. To reduce the common-mode voltage, a multilevel SVPWM has been proposed in . The series SVPWM method has been reported to easily implement SVPWM for the MLCI

In an SVPWM is proposed for hybrid inverters consisting of neutral point clamp and H-bridge inverters to improve output voltage quality and efficiency. As with two-level inverters, it is also possible to implement carrier-based SVPWMs which are equivalent to traditional SVPWMs by injecting a common offset voltage to the three-phase references . In some methods to calculate the offset voltages to achieve the optimal space vector switching sequence are addressed. The performances of a carrier-based PWM and an SVPWM are compared, and a PWM scheme is proposed to obtain an optimal output voltage in the multilevel inverter in.

On the other hand, MLCIs require separated dc links. There-fore, if there is one or more faults present in the dc links in each phase, or if the voltage magnitudes of the dc links are unequal, the output voltage of the MLCI can be unbalanced without proper compensation. To resolve this issue, some studies have been conducted. In , it is shown that the available modulation index is reduced under faulty conditions on switch modules in multilevel inverters, and compensation algorithms are proposed for phase-disposition PWM and phase-shifted (PS) PWM cases. For a STATCOM application, a zero sequence voltage to decouple a three-phase MLCI into three

single-phase MLCIs is applied as well as zero average active power techniques to operate the MLCI under unbalanced source or load conditions. Reference explains why the optimum angles and modulation indexes are necessary to obtain maximum balanced load voltages in the MLCI undergoing a fault on switching modules. A neutral voltage shifting technique has been introduced for balancing the state of charge in the MLCI-based battery energy storage system. In , a duty cycle modification method has been proposed to compensate an output voltage imbalance caused by single-phase power fluctuations. Reference has shown that a zero sequence component helps to obtain the maximum balanced output voltages in a fault condition. In , an offset voltage injection technique is studied to balance the output voltage of the MLCI, but the use of an integrator in the compensation method may reduce dynamic characteristics in applications such as EV motor drives. Recently, the multilevel multiphase feedforward space vector modulation technique called MFFSVM is proposed to compensate the voltage imbalances in MLCIs.

In this paper, a carrier-based PWM strategy to balance line-to-line output voltages and to maximize the linear modulation range where the output voltage can be linearly controlled in the MLCI operating under unbalanced dc-link conditions is proposed. In unbalanced dc-link conditions, the maximum synthesizable voltage in each phase is not uniform. Consequently, the linear modulation range is reduced, and a significant output voltage imbalance may occur as output voltage references increase. In order to analyze the imbalance effect, the voltage vector space for the MLCI is evaluated in detail. From this analysis, the theory behind the output voltage imbalance is explained, and the maximum linear modulation range considering unbalanced dc sources is evaluated. After that, a neutral voltage modulation (NVM) strategy is proposed to achieve output voltage balancing as well as to extend the linear modulation range up to the maximum reachable point in theory. In the proposed method, the neutral voltage reference, which considers a zero sequence voltage to compensate the output voltage imbalance, and an offset voltage to extend the linear modulation range are easily obtained through simple arithmetic calculations. In the proposed method, too large of a dc-link imbalance precludes the output voltages from being balanced. This limitation is also discussed. In addition, a fault-tolerant operation is naturally covered, because the MLCI undergoing an unbalanced dc-link condition can be considered as an MLCI operating under a faulty condition on switch modules. Compared to the existing methods, the proposed strategy is very simple to implement, compensates the output voltage imbalance in real time, and maximizes the voltage utilization of the dc links. Therefore, if this scheme is applied

to applications such as EV traction drive systems, the dynamic characteristics can be greatly improved.

This paper is organized as follows. In Section II, the voltage vector space for the one-by-three configuration MLCI is analyzed for a conceptual study. The proposed modulation strategy is addressed in Section III. In Sections IV and V, the simulations and the experimental results on the two-by-three MLCI are presented. Section VI concludes this paper.

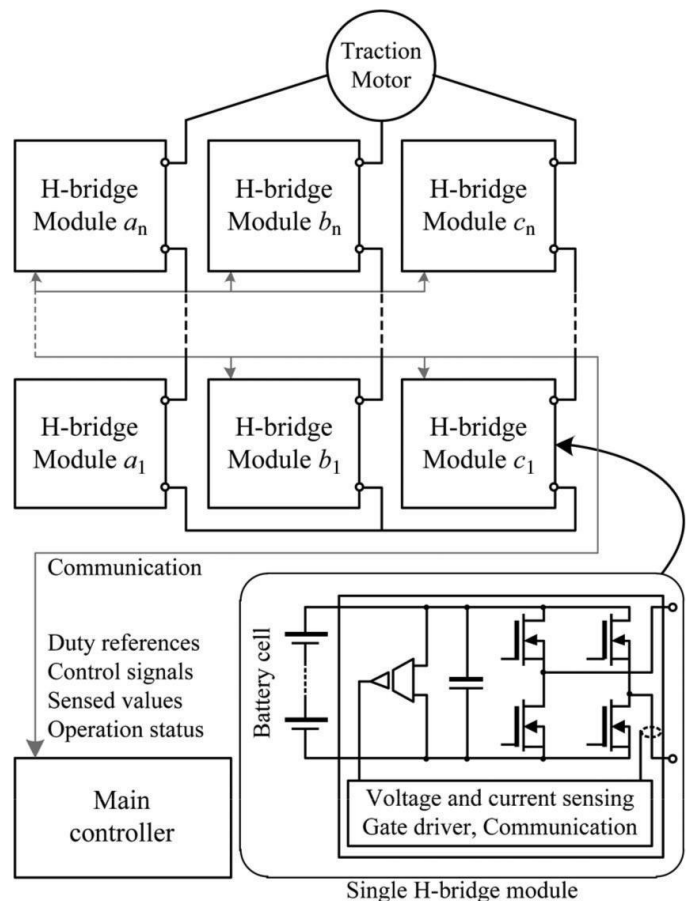


Fig. 1. MLCI-based inverter for EV traction drive.

II. SYSTEM CONFIGURATION AND VOLTAGE

VECTOR SPACE ANALYSIS

A. Configuration of MLCI for EV Traction Motor Drive

Fig. 1 shows the EV traction motor drive system that is dealt with in this paper. In this configuration, various power ratings can be easily implemented by configuring the number of the single H-bridge modules according to a required specification such as a neighborhood EV, full-size sedan, and so on. Here, each H-bridge module incorporates voltage and current sensing circuitries, gate drivers, and communication

interfaces between the module itself and the main controller. In addition, battery cells can be also included in the H-bridge module. The unipolar modulation technique is applied between two switching legs in the H-bridge module. Consequently, the effective switching frequency in each H-bridge module is twice the carrier frequency. In addition to this, the well-known PS modulation technique is used to implement interleaving and multilevel operation. Therefore, the effective switching frequency f_{sw} in a phase is

$$f_{sw} = 2N \times f_c \tag{1}$$

where N and f_c represent the number of the H-bridge modules in each phase and the carrier frequency of PWM, respectively. As an example, Fig. 2 shows the carriers for each module, the duty cycles in unipolar modulation, and the output voltage when $N = 2$.

B. Voltage Vector Space Analysis

When the dc-link voltage of a single H-bridge module is V_{dc} , the output voltage v_{pn} has three states, i.e., V_{dc} , 0, and $-V_{dc}$,

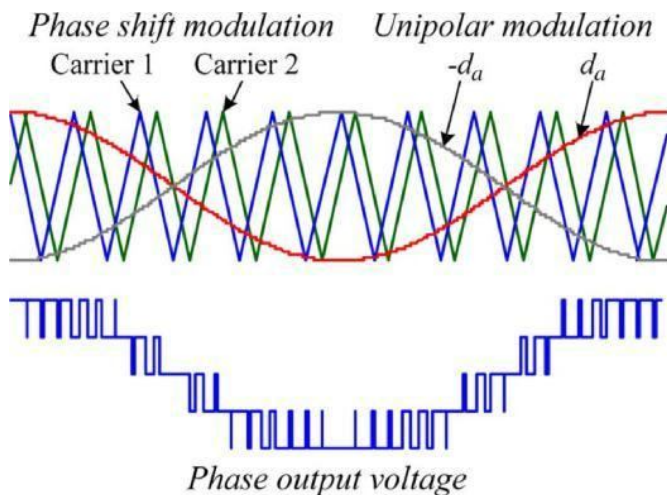


Fig. 2. Unipolar and phase shift modulation for single H-bridge module.

II. MODELING OF STATE SPACE EQUATION OF THE SYSTEM

The general state space model is following that,

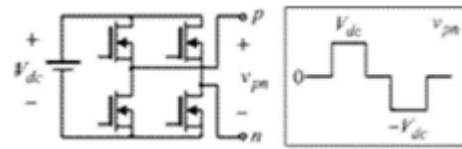


Fig. 3. Output voltage of a single H-bridge module

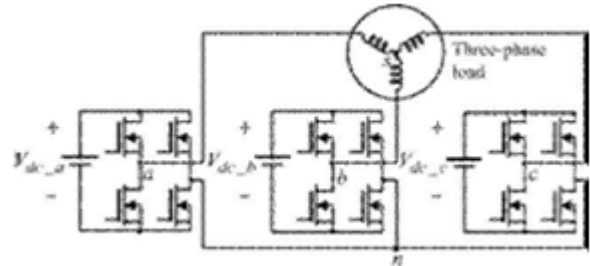


Fig. 4. One-by-three configuration MLCI.

as shown in Fig. 3. By adopting the concept of a switching function, it can be represented as

$$v_{pn} = S_p V_{dc} \tag{2}$$

$S_p \in \{-1, 0, 1\}$ $p=a, b, c$

where S_p is a switching function and p can be replaced with a, b , or c , which represent the phases.

Fig. 4 shows a simple one-by-three configuration MLCI. For voltage vector space analysis, the main concept is derived from this simple topology, and then, it is expanded to more levels. In Fig. 4, there are two neutral points s and n in the MLCI. Here, the voltage between the output point of each phase and the neutral point n is defined as the pole voltage. The pole voltages are represented as v_{an} , v_{bn} , and v_{cn} . The voltage between the output point of each phase and the load side neutral point s is specified as the phase voltage. The phase voltages include v_{as} , v_{bs} , and v_{cs} . By using this concept, the voltage between the two neutral points is defined as v_{sn} and can be written as

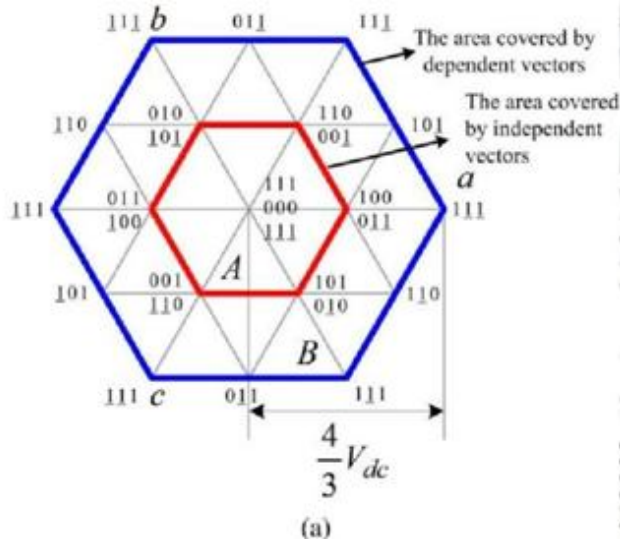
$$v_{sn} = -v_{as} + v_{an} = -v_{bs} + v_{bn} = -v_{cs} + v_{cn} \tag{3}$$

By using the condition that the sum of all phase voltages is zero because the load does not have a neutral line, v_{sn} is rewritten as

$$v_{sn} = \frac{1}{3}(v_{an} + v_{bn} + v_{cn}) \tag{4}$$

$$\dot{x} = Ax + Bu \dots\dots\dots (2.1)$$

$$y = Cx + D \dots\dots\dots (2.2)$$



$$v_{as} = \frac{2}{3} S V_a - \frac{1}{3} S V_b - \frac{1}{3} S V_c$$

$$v_{bs} = -\frac{1}{3} S V_a + \frac{2}{3} S V_b - \frac{1}{3} S V_c$$

$$v_{cs} = -\frac{1}{3} S V_a - \frac{1}{3} S V_b + \frac{2}{3} S V_c \quad (5)$$

If the magnitudes of three dc links are balanced so that V_{dc_a} , V_{dc_b} , and V_{dc_c} have the same value V_{dc} , the voltage vector space in α - β coordinates is defined in Fig. 5(a) by using (5). In the figure, underbars indicate that the switching function has the value of -1 . A part of the hexagon in Fig. 5(a) is shown in Fig. 5(b). In this figure, the vectors $v_{0\bar{1}0}$ and $v_{1\bar{1}\bar{1}}$ are placed at the same reference axis, phase b . However, the constituents of those vectors are different. For $v_{0\bar{1}0}$, this vector can be synthesized without the other two phases' assistance. However, $v_{1\bar{1}\bar{1}}$ cannot be produced without other vectors according to (5). From this, let the vectors which do not require other two phases' assistance to be defined as "the independent vectors." Similarly, the vectors which require other phases' support are defined as "the dependent vectors." According to these definitions, v_{100} , v_{001} , and $v_{0\bar{1}0}$ are the independent vectors, while $v_{1\bar{1}\bar{1}}$, $v_{1\bar{1}1}$, and $v_{1\bar{1}\bar{1}}$ are the dependent vectors in Fig. 5(b). Fig. 5(a) also compares the regions that can be composed by the independent

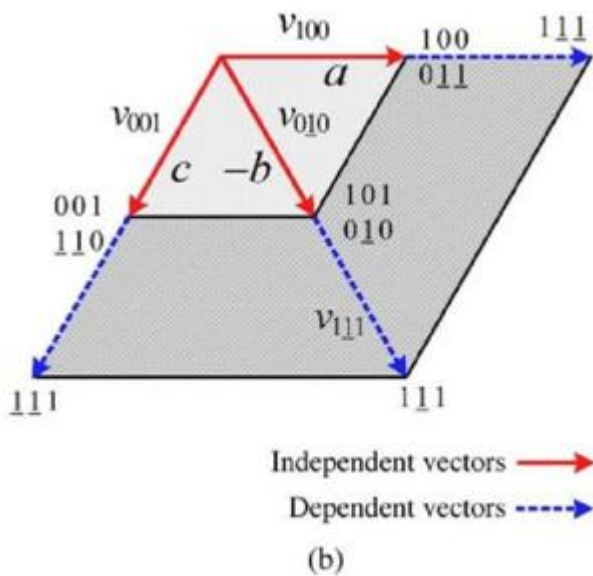


Fig. 5. Voltage vector space of one-by-three configuration MLCI.

By substituting (4) into (3), the phase voltage of each phase is represented as follows by using the relationship defined in (2):

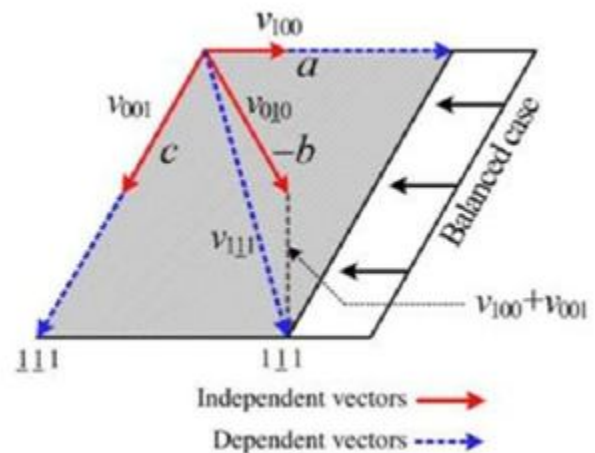


Fig. 6. Voltage vector space in an unbalanced dc-link condition.

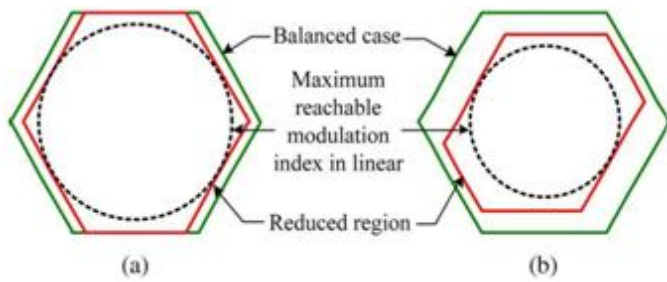


Fig. 7. Comparison of the voltage vector space under different dc-link ratios.

$$(a) V_{dc_a} < V_{dc_b} = V_{dc_c}, (b) V_{dc_b} < V_{dc_a} < V_{dc_c}$$

the dependent vectors. Unlike traditional three-phase half-bridge inverters, the independent vectors can be fully applied in a switching period because the dc links in each of the three phases are separated in the given system. It should be noted that the maximum voltage is decided by the dependent vectors in the entire voltage vector space.

Now, let us consider the case when a three-phase load is supplied by unequal dc links. Fig. 6 shows an extremely unbalanced case where V_{dc_a} is half of the others. If V_{dc_a} decreases, the magnitudes of the independent vectors in phase a are also reduced. As a result, the magnitude of v_{100} is decreased. Here, the phase angle of v_{111} , which is the sum of v_{010} , v_{100} , and v_{001} , is no longer matched with the angle of the independent vectors in phase b from the figure. As shown in the figure, if the magnitudes of the independent vectors are reduced, the available voltage vector space is also reduced, and the angles of the dependent vectors are no longer multiples of 60° . Using these properties, the voltage vector spaces in two different cases are compared in Fig. 7. In Fig. 7(a), V_{dc_a} has a lower value than the others. In Fig. 7(b), all three dc links have different voltages. As it can be seen in Fig. 7, the original shape of the hexagon is distorted in both cases. This means that the trajectory of the maximum output voltage vector in the $\alpha-\beta$ coordinates is also distorted according to the shape of the hexagon in each. On the other hand, the magnitude of the maximum modulation index in the linear modulation range in a given hexagon corresponds to the radius of the inner circle which is inscribed in the hexagon. As shown in Fig. 7, the radius is changed as the hexagon distorts, and the achievable linear modulation range is also altered. Here, the maximum amplitude of the phase voltage V_{ph_max} in the linear modulation range is defined as

$$V_{ph_max} = V_m \frac{\sqrt{3}}{2} \quad (6)$$

$$V_{dc_max} = \frac{2 V_{dc_max} V_{dc_mid}}{V_{dc_max} + V_{dc_min}}$$

Voltage limitation from the medium dc link Voltage limitation from the minimum dc link

where V_{dc_max} , V_{dc_mid} , and V_{dc_min} represent the maximum, medium, and minimum voltages among the dc links. In fact, (6) can be simplified as

$$V_{ph_max} = \frac{V_{dc_mid} + V_{dc_min}}{\sqrt{3}} \quad (7)$$

It should be noted that V_{ph_max} is the maximum synthesizable voltage in the linear modulation range in the MLCI undergoing unbalanced dc-link conditions. From (7), it can be recognized that V_{ph_max} is determined by V_{dc_mid} and V_{dc_min} . If all dc links are well balanced so that V_{dc_mid} and V_{dc_min} have identical values, (7) is rewritten as

$$V_{ph_max} = \sqrt{\frac{2}{3}} V_{dc} \quad (8)$$

This is exactly double the maximum synthesizable voltage in the linear modulation range of a traditional three-phase half-bridge inverter. In fact, the inverter in Fig. 4 is considered as a three-phase full-bridge inverter which is fed by independent dc links. To extend the proposed approach to the multistage MLCI using PS modulation, the total dc-link voltage per phase is represented as

$$V_{dc_p} = \sum_{j=1}^N V_{dc_p(j)} \quad p=a, b, \text{ or } c \quad (9)$$

where p represents a certain phase among phases a , b , and c , N is the number of the power stage modules in each phase, and j represents the index of a power stage module in each phase. In the multistage MLCI, (9) is utilized to obtain V_{dc_max} , V_{dc_mid} , and V_{dc_min} . After that, (7) is still applied.

III. PROPOSED MODULATION TECHNIQUE

In Section II, the maximum synthesizable voltage in the linear modulation range was evaluated under the unbalanced dc links. In this section, a method is proposed to realize the maximum modulation index in the linear modulation range under these conditions.

A. Traditional Offset Voltage Injection Method

The offset voltage injection scheme is a popular technique in three-phase half-bridge inverter applications. The theory behind this is that an offset voltage is incorporated with phase voltage

If the dc links in an MLCI are unbalanced and the traditional offset voltage injection methods are utilized, the three-phase output voltages may become distorted as the phase voltage reference approaches V_{ph_max} . This is because the traditional methods are not considering unbalanced dc-link conditions. Therefore, even if a phase can synthesize an output voltage reference in the linear modulation range, the other phases can be saturated or go into the overmodulation region. In this situation, a neutral voltage can be produced by the saturated or overmodulated phase. In order to resolve this issue and to synthesize the output voltage to V_{ph_max} in the linear modulation range, the NVM technique is proposed in this paper. Fig. 8 shows the concept of the proposed NVM technique. Here, a neutral voltage between the two neutral points n and s in Fig. 4 is modulated to compensate the output voltage imbalance caused by unbalanced dc-link conditions. To do this, first, the weight constant K_w is defined as

$$K_w = \frac{V_{dc_mid} + V_{dc_min}}{2} \tag{12}$$

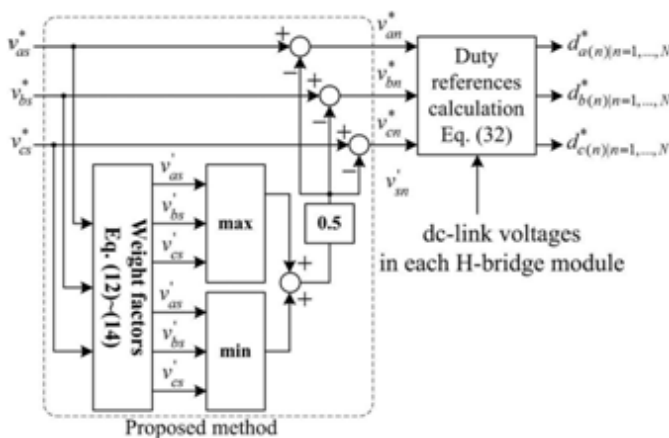


Fig. 8. Implementation of the NVM method

references to implement various PWM schemes in carrier-based PWM by using the fact that line-to-line voltages are applied to a three-phase load [43], [44]. For example, the offset voltage v_{sn}^* is injected to the phase voltage references v_{as}^* , v_{bs}^* , and v_{cs}^* to implement carrier-based SVPWM as in

$$v_{sn}^* = \frac{V_{as}^* + V_{bs}^*}{2} \tag{10}$$

$$V_{max}^* = \max(V_{as}^*, V_{bs}^*, V_{cs}^*)$$

$$V_{min}^* = \min(V_{as}^*, V_{bs}^*, V_{cs}^*)$$

Then, the pole voltage references v_{an}^* , v_{bn}^* , and v_{cn}^* , which will be converted to PWM duty references, are

$$v_{an}^* = V_{as}^* - v_{sn}^* \quad v_{bn}^* = V_{bs}^* - v_{sn}^* \quad v_{cn}^* = V_{cs}^* - v_{sn}^* \tag{11}$$

However, the aforementioned technique may not maximize the linear modulation range in MLCI undergoing unbalanced dc-link conditions.

B. Proposed NVM Method

By using (12), the weight factors are calculated as

$$K_{w_a} = \frac{K_w}{V_{dc_a}}, \quad K_{w_b} = \frac{K_w}{V_{dc_b}}, \quad K_{w_c} = \frac{K_w}{V_{dc_c}} \quad (13)$$

where K_{w_a} , K_{w_b} , and K_{w_c} represent the weight factors for phases a , b , and c , respectively. Next, the weight factors are multiplied by the phase voltage references, and the new references v_{as} , v_{bs} , and v_{cs} are obtained as

$$v_{as} = K_{w_a} v_{as}^*, \quad v_{bs} = K_{w_b} v_{bs}^*, \quad v_{cs} = K_{w_c} v_{cs}^* \quad (14)$$

It should be noted that, depending on dc-link conditions, the sum of v_{as} , v_{bs} , and v_{cs} may not be zero. By using these components, the injected voltage v_{sn} and the pole voltage references are given as

$$v_{max} = \max(v_{as}, v_{bs}, v_{cs}), \quad v_{min} = \min(v_{as}, v_{bs}, v_{cs})$$

$$\frac{v_{max}}{v_{max} + V_{dc}} \quad \frac{v_{min}}{v_{min} - V_{dc}}$$

$$v_{cn}^* = v_{cs}^* - v_{sn}$$

From (15), the line-to-line voltages across each phase of the load are represented as

$$v_{bc}^* = v_{bn}^* - v_{cn}^* = v_{bs}^* - v_{sn} - v_{cs}^* + v_{sn}$$

$$v_{ca}^* = v_{cn}^* - v_{an}^* = v_{cs}^* - v_{sn} - v_{as}^* + v_{sn}$$

$$= \frac{v_{as}^* - v_{bs}^*}{2} - v_{cs}^* - v_{as}^* \quad (16)$$

As it can be seen in (16), v_{sn} does not appear in the line-to-line voltages, and it is still considered as a hidden freedom of voltage modulation. Now, let us consider the role of the weight factors K_{w_a} , K_{w_b} , and K_{w_c} , which are inversely proportional to the corresponding dc-link voltage. For convenience, let us assume that the magnitudes of the dc-link voltage are under the following relationship:

$$V_{dc_a} < V_{dc_b} < V_{dc_c} \quad (17)$$

Then, from (13) and (17)

$$K_{w_a} > K_{w_b} > K_{w_c} \quad K_{w_a} > 1$$

$$K_{w_b}, K_{w_c} < 1. \quad (18)$$

Equation (18) gives

$$|v_{as}| > |v_{bs}| > |v_{cs}| \quad |v_{cs}| < |v_{cs}^*| \quad (19)$$

From (15) and (19), it can be recognized that, if v_{as} , whose dc-link voltage is less than the others, is corresponding to v_{max} or v_{min} , the absolute value of v_{sn} is greater than v_{sn}^* in (10). On the other hand, the final pole voltage references v_{an}^* , v_{bn}^* , and v_{cn}^* are calculated by subtracting v_{sn} from the original phase voltage references v_{as}^* , v_{bs}^* , and v_{cs}^* as in (15). From this reasoning, in this example, it is supposed that, if v_{as} is corresponding to v_{max} , then the final pole voltage references v_{an}^* , v_{bn}^* , and v_{cn}^* are less than the original pole voltage references

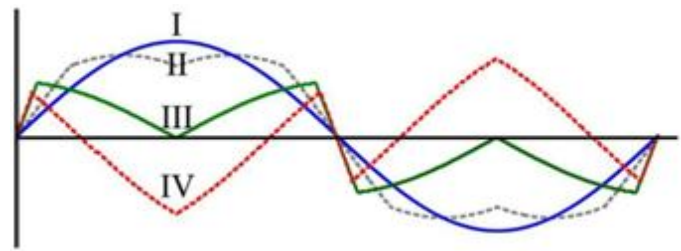


Fig. 9. Comparison of modulated waveforms. (I) Without v_{sn}^* . (II) Traditional carrier-based SVPWM. (III) Proposed NVM with $V_{dc_a} = 0.275 V_{dc}$,

$V_{dc_b} = V_{dc}$, and $V_{dc_c} = V_{dc}$. (IV) Proposed NVM with $V_{dc_a} = 0.2 V_{dc}$, $V_{dc_b} = V_{dc}$, and $V_{dc_c} = V_{dc}$.

which are not considering v_{sn} but v_{sn}^* . On the contrary, if v_{cs} is v_{max} , then the final pole voltage references are greater than the original pole voltage references. By using this principle, the proposed method reduces the portion of the phase whose dc-link voltage is smaller than the others and increases the utilization of the phase in which the dc-link voltage is greater than those of the other phases. However, as it can be seen in (16), v_{sn} does not affect the line-to-line voltages. Therefore, the line-to-line voltage is the same as the one derived from the original phase voltage reference. From this analysis, the proposed method enables the maximum synthesizable modulation index in the linear modulation range under the unbalanced dc-link conditions to be achieved. In addition to this, if all of the dc-link voltages are well balanced so that V_{dc_a} , V_{dc_b} , and V_{dc_c} are equal to V_{dc}

$$V_{dc_{mid}} = V_{dc_{min}} = V_{dc}$$

By substituting (20) into (12)–(14)

$$K_w = \frac{V_{dc_{mid}} + V_{dc_{min}}}{2} = V_{dc} \quad (20)$$

$$K_{w_a} = K_{w_b} = K_{w_c} = 1$$

$$v_{as} = v_{as}^*, \quad v_{bs} = v_{bs}^*, \quad v_{cs} = v_{cs}^* \quad (21)$$

Equation (21) shows that the proposed method gives the same voltage references as the traditional method under balanced dc-link conditions.

C. Constraints of the Proposed Method

In this section, the limitation of how unbalanced dc links can be while still being compensated by the proposed

method is evaluated. Fig. 9 shows the modulated voltage waveforms with different modulation methods and dc-link conditions. In the figure, cases I and II show the results of traditional sinusoidal PWM (SPWM) and carrier-based SVPWM, while cases III and IV illustrate the waveforms of the proposed method with different ratios of dc-link voltages. The fundamental idea to examine the limitation of the proposed method is to evaluate what conditions bring the different polarities between the original voltage reference and the modified voltage reference by using the proposed method. In Fig. 9, the vertices at $\pi/2$ and $3\pi/2$ rad

$$\begin{aligned}
 d^* = d^* &= \dots = d^* = \frac{V^*}{V_{dc_a}} \\
 a1 \quad a2 \quad \dots \quad aN \\
 d^* = d^* &= \dots = d^* = \frac{v^*}{V_{dc_b}} \\
 b1 \quad b2 \quad \dots \quad bN \\
 d^* = d^* &= \dots = d^* = \frac{v^*}{V_{dc_c}} \\
 c1 \quad c2 \quad \dots \quad cN
 \end{aligned} \tag{32}$$

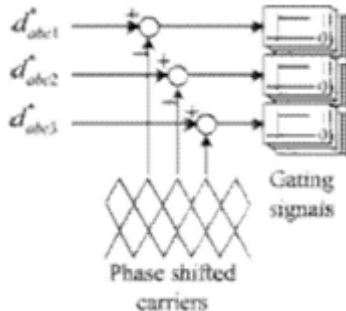


Fig. 10. Comparison of the duty references and the carriers.

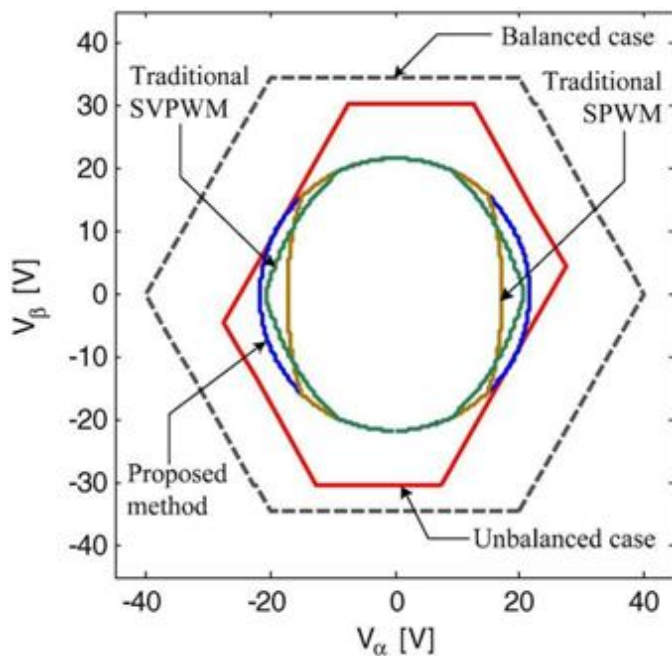


Fig. 11. Comparison of the voltage vector trajectories.

D. Duty Calculation

In Fig. 8, the final voltage references are entered to the duty reference calculation block. In this block, the duty references of each H-bridge module are calculated as follows:

The calculated duty references are compared to PS carriers to generate gating signals, as shown in Fig. 10. It should be noted that the duty references for each H-bridge in each phase are shared in the PS modulation.

IV. MATLAB DESIGN OF CASE STUDY AND RESULTS

A simple one-by-three configuration MLCI model is built in Matlab & Simulink. The three-phase RL load with $R = 0.1$ ohms and $L = 1mH$ is employed and results as shown in Figs.6 to 8. The dc-link voltages for each phase are $V_{dc_a} = 0.3 \times 30$ V, $V_{dc_b} = 0.73 \times 30$ V, and $V_{dc_c} = 30$ V. From (7), the maximum synthesizable phase voltage in linear is Fig. shows the time-domain simulation results with the same simulation condition. From $t = 0.0$ s to $t = 0.05$ s, traditional SPWM is used. From $t = 0.05$ s to $t = 0.1$ s, traditional SVPWM is used. After $t = 0.1$ s, the proposed method is applied. When traditional SPWM is applied, v_{sn} is zero, and the pole voltage references are Figure 6. Output waveform of traditional SPWM, traditional SVPWM, and the proposed method. identical to the ones in (12). With traditional SVPWM, v_{sn} is no longer zero, and the peak voltage of the pole voltage references is reduced compared to SPWM. However, the duty reference of phase a, where the dc-link voltage is minimum among the three phases, is saturated in both cases. Whereas with the proposed method, the fundamental frequency component of the neutral voltage is included in v_{sn} , and the duty references are not saturated. The benefit of the proposed method can also be observed from the peak value of the phase current in the last section of the figure. Under traditional methods, the phase currents are unbalanced. However, the phase currents are well balanced with the proposed method. From the simulation results, it can be seen that the proposed method cansynthesize the maximum available phase voltage in the linear modulation range under unbalanced dc-link. The simulation results for SPWM, SVPWM and PROPOSED METHOD are concluded using MATLAB.

Design and simulation of SVMW and PROPOSED METHODS as below figures.

Fig.12. Simulink model of proposed method

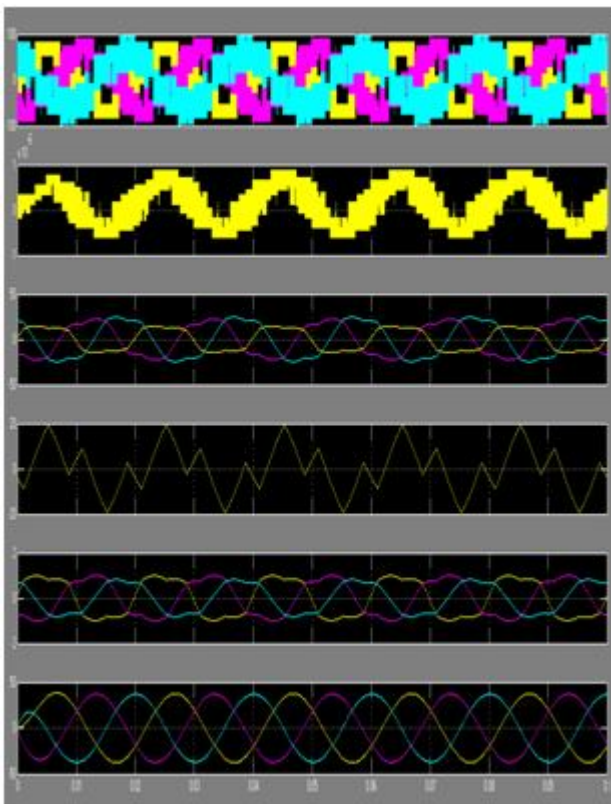


Fig.13. Simulation results of proposed method

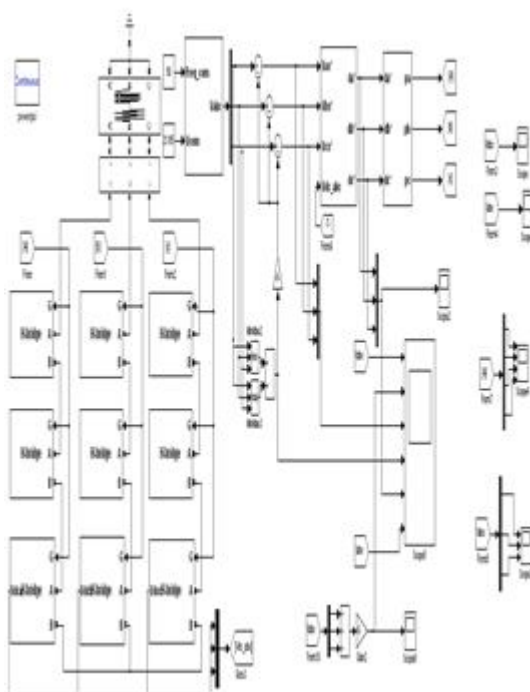


Fig.14. Simulink model of conventional SVPWM technique

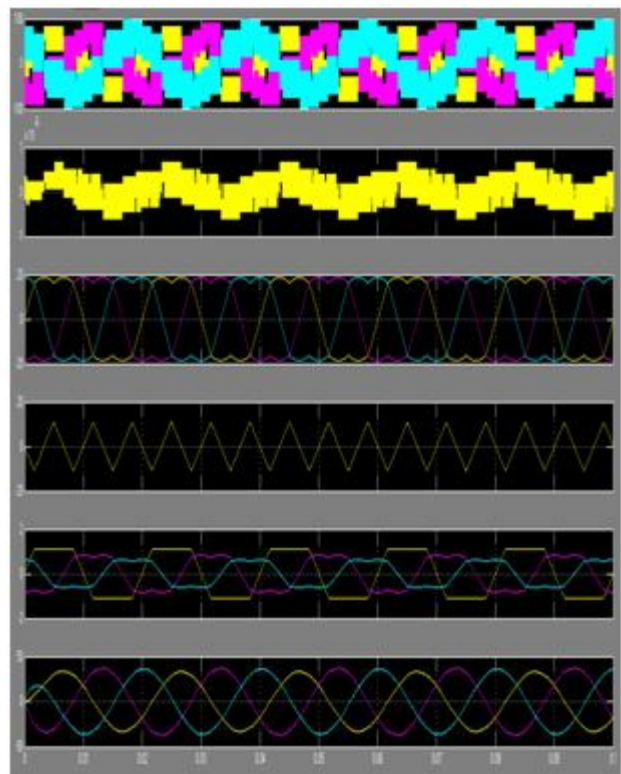


Fig.15. Performance of conventional SVPWM technique

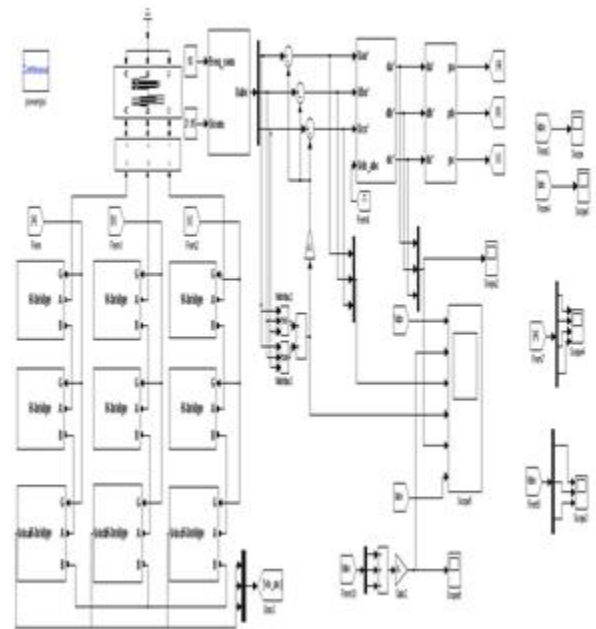


Fig.16. Simulink model of conventional traditional SPWM technique

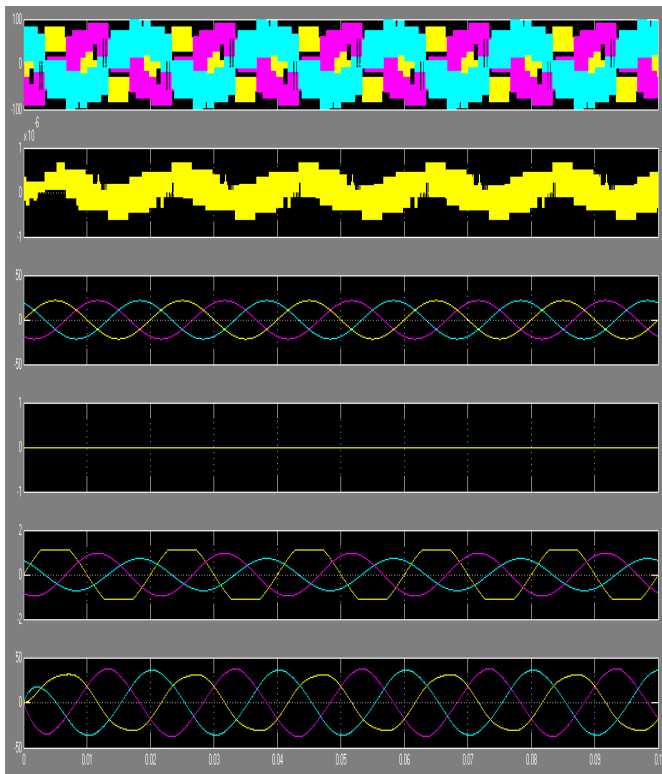


Fig.17.Performance of traditional SPWM.

VI. CONCLUSION

The NVM technique for MLCIs under unbalanced dc-link conditions has been proposed in this paper. In order to analyze the maximum synthesizable voltage of MLCIs, the voltage vector space has been analyzed using the switching function. From the analysis, the maximum linear modulation range was derived. The proposed NVM technique is applied to achieve the maximum modulation index in the linear modulation range under an unbalanced dc-link condition as well as to balance the output phase voltages. Compared to the previous methods, the proposed technique is easily implemented and improves the output voltage quality under unbalanced dc-link conditions. Both simulations and experimental results based on the IPM motor drive application verify the effectiveness of the proposed method.

REFERENCES

- [1] J. Rodriguez, J.-S. Lai, and F. Z. Peng, "Multilevel inverters: A survey of topologies, controls, and applications," *IEEE Trans. Ind. Electron.*, vol. 49, no. 4, pp. 724–738, Aug. 2002.
- [2] H. Abu-Rub, J. Holtz, J. Rodriguez, and G. Baoming, "Medium-voltage multilevel converters—State of the art, challenges, and requirements in industrial applications,"

IEEE Trans. Ind. Electron., vol. 57, no. 8, pp. 2581–2596, Aug. 2010.

- [3] J.-S. Lai and F. Z. Peng, "Multilevel converters—A new breed of power converters," *IEEE Trans. Ind. Appl.*, vol. 32, no. 3, pp. 509–517, May/Jun. 1996.
- [4] M. Malinowski, K. Gopakumar, J. Rodriguez, and M. A. Perez, "A survey on cascaded multilevel inverters," *IEEE Trans. Ind. Electron.*, vol. 57, no. 7, pp. 2197–2206, Jul. 2010.
- [5] J. Rodriguez, L. G. Franquelo, S. Kouro, J. I. León, R. C. Portillo, A. M. Prats, and M. A. Perez, "Multilevel converters: An enabling technology for high-power applications," *Proc. IEEE*, vol. 97, no. 11, pp. 1786–1817, Nov. 2009.